


Ultrafast Ratchet Dynamics of Skyrmions by Defect Engineering in Materials with Poor Conductivity Under Gigahertz Magnetic Fields

Weijin Chen^{1,2,3}, Linjie Liu^{2,3} and Yue Zheng^{2,3,*}

¹*School of Materials, Sun Yat-sen University, 510275 Guangzhou, China*

²*State Key Laboratory of Optoelectronic Materials and Technologies, Sun Yat-sen University, 510275 Guangzhou, China*

³*Micro&Nano Physics and Mechanics Research Laboratory, School of Physics, Sun Yat-sen University, 510275 Guangzhou, China*

 (Received 6 May 2020; revised 8 October 2020; accepted 16 November 2020; published 3 December 2020)

The ratchet motion of magnetic skyrmions driven by microwave magnetic fields, with the motion direction and speed tunable by field parameters, provides a promising route to drive magnetic skyrmions in materials with poor conductivity. However, as an indirect motion, skyrmion ratchet-motion speed is generally low in comparison with the direct motions driven by currents. Toward practical applications, it is necessary to ask if there are mechanisms to realize ultrafast ratchet motion of magnetic skyrmions and how such a motion can be integrated into racetrack-type skyrmion devices. In this work, we explore the effects of defects and edges on the ratchet motion of magnetic skyrmions under time-varying magnetic fields in GHz. We demonstrate that the ratchet motion of skyrmion is not only guided along the defect tracks or edges, but also with a remarkable speed up (with a factor over 10) compared with that in the bulk region. The skyrmion ratchet-motion speed reaches 100 m/s along a straight defect track and edge and 10^9 rad/s along a circular edge under a field of approximately 50 mT, comparable to those direct motions driven by currents. Moreover, the skyrmion ratchet motion along the defect track or edge can be facily controlled by the field and defect parameters. Analysis based on the time-averaged Thiele equation of skyrmion verifies that such a speed-up effect is due to the increased time-averaged driving force perpendicular to the skyrmion motion when it approaches the defect track or edge, analogous to that discovered in direct motions driven by currents. The generality of our conclusions has been examined for the ratchet motion of Bloch and Néel-type skyrmions driven by a variety of time-varying magnetic fields, and for systems with open edges or defect tracks with modified Dzyaloshinskii-Moriya or exchange interactions and anisotropy.

DOI: [10.1103/PhysRevApplied.14.064014](https://doi.org/10.1103/PhysRevApplied.14.064014)

I. INTRODUCTION

Magnetic skyrmions are a kind of particlelike chiral spin structures with a nontrivial topological feature (i.e., cannot be continuously “unwound” to a ferromagnetic or other magnetic state). They resemble magnetic vortices and bubbles in many aspects but can have a much smaller size down to several nanometers [1–3]. Magnetic skyrmions have been experimentally observed in both metallic and poorly conductive materials with Dzyaloshinskii-Moriya (DM) interaction, caused by a breaking of inversion symmetry in the crystal lattice [4–9] or nearby the interfaces [10–16]. Their relatively small sizes, robust metastability, as well as the intriguing dynamics and transport properties under external sources, make magnetic skyrmions appealing building blocks in ultradense information storing and

processing devices. Particularly, the concepts of racetrack-type devices are improved by skyrmions, and the threshold current to displace magnetic skyrmions is rather low compared with magnetic domain walls, implying the potential of developing highly energy-efficient devices.

An in-depth understanding of skyrmion motion characteristics is crucial for their promising applications. It is a well-known fact that magnetic skyrmions can be displaced, e.g., by spin-polarized currents via the spin-transfer torque (STT) or spin-orbit torque (SOT) applicable for metallic systems [17–19], and by field or field gradients in the absence of spin torques from the conduction electrons applicable for both metallic and insulating systems [20–28]. The nontrivial topology of skyrmions manifests itself in the motion known as the skyrmion Hall effect (SkHE) [29,30], a reverse effect of the topology-induced emergent fields acting on conduction electrons and magnons. The SkHE would drive skyrmions to the edges of the system and causes possible annihilation, limiting the maximum

*zhengy35@mail.sysu.edu.cn

velocity of skyrmion. Meanwhile, when skyrmion is moving along the edge, a speed-up effect occurs due to the repulsive force of the edge [31,32]. So far, a lot of efforts have been paid to pursue high-speed and controllable motion of skyrmions. In particular, researchers have proposed the use of racetrack-type structures (e.g., narrow stripes with natural edges or defect tracks with different anisotropy, DM or exchange interactions from those of the surroundings) to guide the motion of skyrmion [18,19,32–35]. With the further use of antiferromagnetic bilayer structures [36], low-symmetry heavy-metal substrates [37] or ferrimagnetic materials [38], the SkHE can be largely suppressed and the speed limit in skyrmion racetrack devices driven by currents can be overcome by a factor of 10 [37].

While the academic focus has been put on the direct motion of skyrmion driven by time-unvarying sources, some works have shown that a net motion of skyrmion can also be realized by indirect motions under time-varying

sources [25–27,39–41]. Such motions, occurring in systems with space or time asymmetries, are relevant to general kinds of transport phenomena of solitons, named the ratchet effect. Remarkably, both the speed and the direction of the skyrmion ratchet motions under time-varying magnetic fields can be tuned by the field parameters [26,41]. This indicates a general and feasible strategy to drive skyrmions in both conductive and insulating materials. Particularly, magnetic insulators that host skyrmions (e.g., Cu_2OSeO_3 and $\text{Y}_3\text{Fe}_5\text{O}_{12}$) are attractive since they have very low damping and allow long-distance information transmission free of Joule heating. The skyrmion ratchet motion driven by magnetic fields provides a way to transport the skyrmions in magnetic insulators, where current driving is not favored. Nevertheless, being an indirect motion, the skyrmion ratchet-motion speed is generally low compared with the direct motions driven by currents, despite the fact that a relatively fast ratchet motion can be realized via a trade-off of stability for

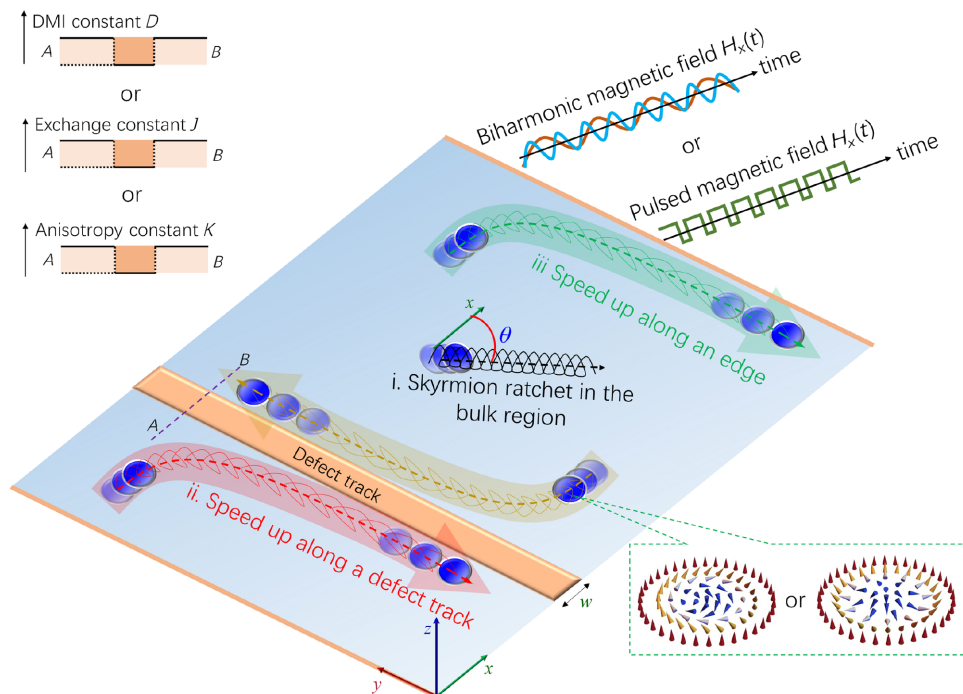


FIG. 1. Schematic illustrations of the physical model and the basic idea of defect-induced ultrafast ratchet motion of skyrmion under time-varying magnetic fields. Analogy to other soliton systems, both Bloch and Néel-type magnetic skyrmions will be driven into ratchet motions by time-varying forces with temporal asymmetry, e.g., in-plane biharmonic magnetic fields $H_x(t) = H_0[\sin(m\omega t) + \sin(n\omega t + \varphi)]$ with m and n being two coprime integers and $m + n$ being odd, or in-plane pulsed magnetic fields with positive pulses and negative pulses in different magnitudes or widths. In the bulk region (i.e., free of defects or edges), the speed of such ratchet motions is relatively low, though a continuous control of speed and direction of such ratchet motions can be achieved by tuning the field parameters (e.g., the frequency ω , phase φ and strength H_0 of the biharmonic field, width of the pulsed field, etc.). When the skyrmion approaches a defect track (with a different DMI, exchange or anisotropy from that of the bulk region) or an edge, it will be guided along the defect track or edge and the skyrmion ratchet motion exhibits a remarkable speed up in comparison with that in the bulk region, due to the remarkably increase of the time-averaged driving force perpendicular to the skyrmion motion when it approaches the defect track or edge. Furthermore, the skyrmion ratchet-motion speed and direction along the defect track or edge can be facilely controlled by the field and defect parameters.

speed (e.g., by increasing the driving-field strength or setting the driving-field frequency close to the resonance frequency of skyrmion [26,41]). At present, strategies to efficiently drive magnetic skyrmions in poor conductive materials are still lacking. Toward practical applications, it is necessary to ask if there are mechanisms to realize ultrafast ratchet motion of skyrmions and how such a motion can be integrated into racetrack-type skyrmion devices.

Based on massive micromagnetic simulations and analytical modeling, this work explores the effects of defects and edges on the ratchet motion of magnetic skyrmions driven by gigahertz magnetic fields and demonstrates a general mechanism of ultrafast ratchet motion (over 100 m/s under a field of approximately 50 mT) of magnetic skyrmions via defect engineering. The physical model and the basic idea of defect-induced ultrafast ratchet motion of skyrmion are schematically illustrated in Fig. 1. We consider a ratchet motion of skyrmion driven by GHz magnetic fields with a temporal asymmetry [41], but our conclusions should not be limited to such a ratchet motion. Two types of driving fields with a temporal asymmetry are focused: in-plane biharmonic magnetic fields $H_x(t) = H_0[\sin(m\omega t) + \sin(n\omega t + \varphi)]$ with m and n being two coprime integers and $m + n$ being odd, and in-plane pulsed magnetic fields with positive pulses and negative pulses in different magnitudes or widths. Due to the temporal asymmetry of the driving fields, skyrmion can be driven into a net motion even though the time average of driving fields is zero and the system is without any space asymmetry. In the bulk region where the skyrmion is far away from defect tracks or edges, the skyrmion would show ratchet motions with a relatively low speed compared with that near the defect tracks or edges [41]. When the skyrmion approaches a defect track or an edge, it will be guided along the defect track or edge and the skyrmion ratchet motion exhibits a much larger speed than that in the bulk region. Analogous to the mechanism discovered in direct motions driven by currents [31,35], the speed-up effect of skyrmion ratchet motion can be explained by a repulsive effective driving force (in a time-averaging view) subjected by the near defect track or edge. We show that the skyrmion ratchet-motion speed and direction along the defect track or edge can be facilely controlled by the field and defect parameters. Our conclusions are general for the ratchet motion of Bloch and Néel-type skyrmions driven by time-varying magnetic fields in systems with open edges or defect tracks (i.e., with modified Dzyaloshinskii-Moriya or exchange interactions and anisotropy). The reported ratchet motion of skyrmion driven by magnetic fields thus may provide an energetically efficient method to control skyrmions because the spin waves (magnons) in an insulating system cause only negligible Joule heat loss compared with the current-driven approach in metallic systems.

II. METHODS

A. Micromagnetic simulation

Based on a Heisenberg model on a two-dimensional (2D) square lattice, we write the following effective Hamiltonian of a chiral magnet as [42]

$$\begin{aligned} \mathcal{H}(\mathbf{m}_i) = & -J \sum_{\langle i,j \rangle} \mathbf{m}_i \cdot \mathbf{m}_j \\ & - D \left(\sum_i \mathbf{m}_i \times \mathbf{m}_{i+e_x} \cdot \hat{e}_x + \sum_i \mathbf{m}_i \times \mathbf{m}_{i+e_y} \cdot \hat{e}_y \right) \\ & - \sum_i \mathbf{H}(t) \cdot \mathbf{m}_i - Km_z^2, \end{aligned} \quad (1)$$

where \mathbf{m}_i is the magnetization vector at site i , J is the Heisenberg exchange coefficient, D is the DM interaction coefficient, K is the anisotropy constant, and $\mathbf{H}(t) = \mathbf{H}_0 + \mathbf{h}(t)$ is the external magnetic field, which is the sum of a constant field normal to the plane $\mathbf{H}_0 = (0, 0, H_z)$ and a time-varying in-plane field $\mathbf{h}(t)$.

The dynamics of skyrmion is captured by solving the stochastic Landau-Lifshitz-Gilbert (LLG) equation,

$$\frac{d\mathbf{m}_i}{dt} = -\gamma \{\mathbf{m}_i \times [\mathbf{H}_i^{\text{eff}} + \mathbf{L}_i^{\text{fl}}(t)]\} + \alpha \left(\mathbf{m}_i \times \frac{d\mathbf{m}_i}{dt} \right) \quad (2)$$

or in the equivalent form,

$$\begin{aligned} \frac{d\mathbf{m}_i}{dt} = & -\frac{\gamma}{\alpha^2 + 1} \left(\mathbf{m}_i \times [\mathbf{H}_i^{\text{eff}} + \mathbf{L}_i^{\text{fl}}(t)] + \alpha \mathbf{m}_i \right. \\ & \left. \times \{\mathbf{m}_i \times [\mathbf{H}_i^{\text{eff}} + \mathbf{L}_i^{\text{fl}}(t)]\} \right), \end{aligned} \quad (3)$$

where $\gamma = g\mu_B/\hbar$ is the gyromagnetic ratio, α is the Gilbert damping coefficient, $\mathbf{H}_i^{\text{eff}}$ is the effective magnetic field given by $\mathbf{H}_i^{\text{eff}} = -\partial\mathcal{H}/\partial\mathbf{m}_i$, and $\mathbf{L}_i^{\text{fl}}(t)$ is the stochastic field caused by the effects of a thermally fluctuating environment interacting with \mathbf{m}_i . $\mathbf{L}_i^{\text{fl}}(t)$ satisfies $\langle \mathbf{L}_i^{\text{fl}}(t) \rangle = 0$ and $\langle L_{i\beta}^{\text{fl}}(t)L_{i\lambda}^{\text{fl}}(s) \rangle = \alpha k_B T \gamma^{-1} m^{-1} \delta_{ij} \delta_{\beta\lambda} \delta(t-s)$, where β and λ are Cartesian indices, T is temperature, k_B is the Boltzmann constant, and $m = |\mathbf{m}_i| = |g\mu_B|/\alpha^3$ is the norm of the magnetization vector.

Numerical simulations based on the stochastic LLG equation are performed via an explicit Euler iteration scheme. The size of sample systems is fixed to be 128×128 sites under the periodic boundary condition. In the bulk region, the Heisenberg exchange J is taken to be $J/k_B = 50$ K [22], the strength of the DM interaction coefficient is $D = 0.15J$, and the anisotropy constant K is taken to be zero. The spin turn angle θ in the helical structure is approximately 6° as determined by $\theta = \arctan[D/(\sqrt{2}J)]$ [42]. The Gilbert damping coefficient α is taken to be 0.1. The external magnetic field normal to the plane is fixed to

be $H_z = 0.015$ in units of $J/(g\mu_B)$, which is approximately 0.16 T for g equal to 6.74. The time step is taken to be 0.01, in units of \hbar/J , which is approximately 1.5 fs. In the main text, the time is expressed in the reduced form $\tilde{t} = t/\tau$, with τ being $10^4 \hbar/J \simeq 1.5$ ns. To first obtain the steady skyrmion, the magnetic structure of the spin-lattice system is initially set with a downward magnetization in the center region and with an upward magnetization elsewhere and is relaxed over a sufficiently long time (> 1 ns).

To characterize the skyrmion, we calculate the topological charge density,

$$q = \frac{1}{4\pi} \mathbf{m} \cdot (\partial_x \mathbf{m} \times \partial_y \mathbf{m}) \quad (4)$$

as defined in the continuous form. The total topological charge is then given by

$$Q = \int q dx dy. \quad (5)$$

And the position of skyrmion $\mathbf{R} = (x_c, y_c)$ can be determined by

$$x_c = \frac{\int x q dx dy}{Q}, \quad y_c = \frac{\int y q dx dy}{Q}. \quad (6)$$

B. Analytical model of skyrmion ratchet motion

Consider the steady ratchet motion of skyrmion driven by a periodically oscillating magnetic field. In this case, the skyrmion deforms dynamically, and the conventional Thiele equation based on the rigid-particle model needs to be modified. Following the idea of previous works [22,25], we separate the magnetization field of a skyrmion into a slowly varying part and fast varying part,

$$\mathbf{m}(\mathbf{r}, t) = \mathbf{m}_0 + \mathbf{n}, \quad (7)$$

where \mathbf{m}_0 is the slowly varying part and \mathbf{n} is the fast varying part related to the spin waves (magnons) dynamics, respectively. For simplicity, we make approximations on \mathbf{m}_0 and \mathbf{n} that $\mathbf{m}_0 = \langle \mathbf{m}(\mathbf{r}, t) \rangle$, $\langle \mathbf{n} \rangle = 0$, with $\langle \rangle$ denoting time averaging over a period. Hence, \mathbf{m}_0 is the time average of the skyrmion magnetization over a period. The time dependence of \mathbf{m}_0 captures the net motion of skyrmion, and is related to the time average of the skyrmion position $\langle \mathbf{R}(t) \rangle$ and the time-averaged skyrmion velocity $\mathbf{v} = \langle \dot{\mathbf{R}} \rangle$ as $\mathbf{m}_0 = \mathbf{m}_0 [\mathbf{r} - \langle \mathbf{R}(t) \rangle]$ and $\dot{\mathbf{m}}_0 = -(\mathbf{v} \cdot \nabla) \mathbf{m}_0$.

Substituting the above $\mathbf{m}(\mathbf{r}, t)$ into the LLG equation [see Eq. (2)], one obtains

$$-(\mathbf{v} \cdot \nabla) \mathbf{m}_0 + \dot{\mathbf{n}} = -\gamma \mathbf{m} \times \mathbf{H}_{\text{eff}} + \alpha (\mathbf{m}_0 + \mathbf{n}) \times [-(\mathbf{v} \cdot \nabla) \mathbf{m}_0 + \dot{\mathbf{n}}]. \quad (8)$$

Multiplying $\mathbf{m}_0 \cdot [(\partial \mathbf{m}_0 / \partial x_i) \times \cdot]$ on all the terms of the above equation gives

$$\begin{aligned} & -\mathbf{m}_0 \cdot \left[\frac{\partial \mathbf{m}_0}{\partial x_i} \times (\mathbf{v} \cdot \nabla) \mathbf{m}_0 \right] + \mathbf{m}_0 \cdot \left(\frac{\partial \mathbf{m}_0}{\partial x_i} \times \dot{\mathbf{n}} \right) \\ & = -\gamma \mathbf{m}_0 \cdot \left[\frac{\partial \mathbf{m}_0}{\partial x_i} \times (\mathbf{m} \times \mathbf{H}_{\text{eff}}) \right] \\ & \quad - \alpha \mathbf{m}_0 \cdot \left\{ \frac{\partial \mathbf{m}_0}{\partial x_i} \times [\mathbf{m}_0 \times (\mathbf{v} \cdot \nabla) \mathbf{m}_0] \right\} \\ & \quad + \alpha \mathbf{m}_0 \cdot \left(\frac{\partial \mathbf{m}_0}{\partial x_i} \times \{\mathbf{n} \times [-(\mathbf{v} \cdot \nabla) \mathbf{m}_0]\} \right) \\ & \quad + \alpha \mathbf{m}_0 \cdot \left[\frac{\partial \mathbf{m}_0}{\partial x_i} \times (\mathbf{m} \times \dot{\mathbf{n}}) \right]. \end{aligned} \quad (9)$$

By defining

$$\mathbf{g} = \left[\mathbf{m}_0 \cdot \left(\frac{\partial \mathbf{m}_0}{\partial y} \times \frac{\partial \mathbf{m}_0}{\partial z} \right), \mathbf{m}_0 \cdot \left(\frac{\partial \mathbf{m}_0}{\partial z} \times \frac{\partial \mathbf{m}_0}{\partial x} \right), \mathbf{m}_0 \cdot \left(\frac{\partial \mathbf{m}_0}{\partial x} \times \frac{\partial \mathbf{m}_0}{\partial y} \right) \right] \quad (10)$$

and

$$\overleftrightarrow{\mathbf{d}} = \begin{bmatrix} d_{11} & d_{12} & d_{13} \\ d_{21} & d_{22} & d_{23} \\ d_{31} & d_{32} & d_{33} \end{bmatrix}, \quad d_{ij} = \alpha \frac{\partial m_{0k}}{\partial x_i} \frac{\partial m_{0k}}{\partial x_j}. \quad (11)$$

Equation (9) can be further written as

$$\begin{aligned} \mathbf{g} \times \mathbf{v} + \overleftrightarrow{\mathbf{d}} \cdot \mathbf{v} & = -\gamma \mathbf{m}_0 \cdot \left[\frac{\partial \mathbf{m}_0}{\partial x_i} \times (\mathbf{m} \times \mathbf{H}_{\text{eff}}) \right] \\ & \quad - \mathbf{m}_0 \cdot \left(\frac{\partial \mathbf{m}_0}{\partial x_i} \times \dot{\mathbf{n}} \right) \\ & \quad + \alpha \mathbf{m}_0 \cdot \left(\frac{\partial \mathbf{m}_0}{\partial x_i} \times \{\mathbf{n} \times [-(\mathbf{v} \cdot \nabla) \mathbf{m}_0]\} \right) \\ & \quad + \alpha \mathbf{m}_0 \cdot \left[\frac{\partial \mathbf{m}_0}{\partial x_i} \times (\mathbf{m} \times \dot{\mathbf{n}}) \right]. \end{aligned} \quad (12)$$

The time averages of those terms related to \mathbf{n} and $\dot{\mathbf{n}}$ in the above equation can be neglected. This leads to

$$\mathbf{g} \times \mathbf{v} + \overleftrightarrow{\mathbf{d}} \cdot \mathbf{v} = - \left\langle \gamma \mathbf{m}_0 \cdot \left[\frac{\partial \mathbf{m}_0}{\partial x_i} \times (\mathbf{m} \times \mathbf{H}_{\text{eff}}) \right] \right\rangle. \quad (13)$$

By integrating all the terms of Eq. (13) with space coordinates, one finally obtains

$$\mathbf{G} \times \mathbf{v} + \overleftrightarrow{\mathbf{D}} \cdot \mathbf{v} = \mathbf{F}. \quad (14)$$

The effective force is defined by

$$F_i = \int -\gamma \mathbf{m}_0 \cdot \left(\frac{\partial \mathbf{m}_0}{\partial x_i} \times \langle \mathbf{m} \times \mathbf{H}_{\text{eff}} \rangle \right) dV, \quad (15)$$

where

$$\begin{aligned} \langle \mathbf{m} \times \mathbf{H}_{\text{eff}} \rangle & \simeq \langle A \mathbf{m}_0 \times \nabla^2 \mathbf{m}_0 - D \mathbf{m}_0 \times (\nabla \times \mathbf{m}_0) + \mathbf{m}_0 \times \mathbf{H} \rangle \\ & + \langle A \mathbf{n} \times \nabla^2 \mathbf{n} - D \mathbf{n} \times (\nabla \times \mathbf{n}) + \mathbf{n} \times \mathbf{h}(t) \rangle. \end{aligned} \quad (16)$$

One can see that the effective driving force is mainly contributed by two parts, the one related to \mathbf{m}_0 ,

$$\begin{aligned} \langle \mathbf{m} \times \mathbf{H}_{\text{eff}} \rangle_1 & = \langle A \mathbf{m}_0 \times \nabla^2 \mathbf{m}_0 - D \mathbf{m}_0 \times (\nabla \times \mathbf{m}_0) + \mathbf{m}_0 \times \mathbf{H} \rangle \\ & \quad (17) \end{aligned}$$

and the one related to \mathbf{n} ,

$$\langle \mathbf{m} \times \mathbf{H}_{\text{eff}} \rangle_2 = \langle A \mathbf{n} \times \nabla^2 \mathbf{n} - D \mathbf{n} \times (\nabla \times \mathbf{n}) + \mathbf{n} \times \mathbf{h}(t) \rangle. \quad (18)$$

Note, \mathbf{G} and $\overleftrightarrow{\mathbf{D}}$ in Eq. (14) are the *effective* gyromagnetic vector and the dissipative force tensor defined by the time-averaged magnetization over a period \mathbf{m}_0 , respectively. The effective force related to $\langle \mathbf{m} \times \mathbf{H}_{\text{eff}} \rangle_1$ in Eq. (17) is nonzero due to the difference between the time-averaged magnetization of skyrmion \mathbf{m}_0 during ratchet motion and that at the equilibrium. Here we denote this part of effective force as the “deformation force” $\mathbf{F}_{\mathbf{m}_0}$ since \mathbf{m}_0 is the field of a skyrmion with a steady deformation in reference to that at the equilibrium. Meanwhile, the part of effective force related to $\langle \mathbf{m} \times \mathbf{H}_{\text{eff}} \rangle_2$ in Eq. (18), which we denote as the “dynamic force” $\mathbf{F}_{\mathbf{n}}$, is caused by the fast-varying \mathbf{n} related to the spin waves (magnons) dynamics, with the first term $\langle A \mathbf{n} \times \nabla^2 \mathbf{n} \rangle$ corresponding to magnon currents [22,25]. Values of \mathbf{G} , $\overleftrightarrow{\mathbf{D}}$, and \mathbf{F} can be readily calculated from the micromagnetic simulation. The ratchet motion speed \mathbf{v} can then be analytically obtained by solving Eq. (14).

III. RESULTS AND DISCUSSION

A. Defect-mediated skyrmion ratchet motion under time-asymmetric fields

The ratchet effect under time-asymmetric fields is general for both Bloch and Néel-type magnetic skyrmions as they are identical particles from the viewpoint of topology (see Figs. S1 and S2 within the Supplemental Material [43]). We take the results of Bloch-type skyrmions to illustrate the key idea of this work. Our simulations are performed on a 2D Heisenberg-type spin lattice with

128×128 sites. The temperature-field T - H_z phase diagram of single-skyrmion state of this spin-lattice system is calculated and depicted in Fig. S3 within the Supplemental Material [43]. It shows that, at a given temperature, the single-skyrmion state (i.e., an isolating skyrmion embedded in a ferromagnetic background) can be stabilized at a moderate out-of-plane magnetic field H_z , consistent with previous works [22,23]. In the following, we fix the condition at $T = 0$ K and $H_z = 0.015$ (in unit of $J/g\mu_B$). Such a condition stabilizes a skyrmion with diameter of approximately 60 nm if we consider a typical lattice parameter of $a = 1$ nm. A finite change of temperature and H_z does not change the main conclusions of this work.

We first reveal the defect-mediated ratchet motion of skyrmion under a biharmonic magnetic field $H_x(t) = 0.003 [\sin(\omega t) + \sin(2\omega t)]$ along the x axis. The angular frequency of the fields ω is set to be 105 Grad/s (also in the following). The corresponding frequency is $f = 16.7$ GHz. This value is close to the resonance frequency of the counter-clockwise (CCW) gyration mode of the skyrmion and leads to a relatively fast ratchet motion [41]. Two cases are investigated. For the first case, denoted as “defect track // y ,” the $128a \times 128a$ spin-lattice system is in periodic boundary conditions along both x and y axes, and a $4a$ -wide defect track (with the DM interaction constant being half of that in the bulk region, i.e., $\eta_{\text{DMI}} = 0.5$) parallel to the y axis is located at $x = 96a$. For the second case, denoted as “edge // x ,” the spin-lattice system has a periodic boundary condition along the x axis and an open-circuit condition along the y axis (i.e., there are two edges parallel to the x axis). For both cases, an isolating skyrmion is initially located at the center of the system ($64a, 64a$). The core of skyrmion before motion is far enough from the defect track and edges, therefore the skyrmion motion at the beginning can be considered as that in the bulk region. Figure 2(a) and 2(b) depict the motion trajectories of the skyrmion in the two cases, respectively. It is clearly seen that for both cases the skyrmion exhibits a ratchet motion with a helical trajectory under the biharmonic in-plane magnetic field. At the beginning, the pitches of the helical trajectories of skyrmion for both cases are rather small [see the “no. 1” insets in Figs. 2(a) and 2(b)], indicating a small ratchet speed. As the skyrmion approaches the defect track or the edge, the pitches of the helical trajectories of skyrmion for both cases gradually increase, and become much larger than that in the bulk region when the skyrmion finally moves along the defect track or the edge [see the “no. 2” insets in Figs. 2(a) and 2(b)]. This clearly demonstrates a speed-up effect of the skyrmion ratchet motion caused by the defect track and edge, analogous to that reported in the direct transport of skyrmion driven by currents [31,35].

Such a speed-up effect can be quantitatively inferred from the long-time evolution curves of the skyrmion position coordinates x_c and y_c of the two cases, as shown in

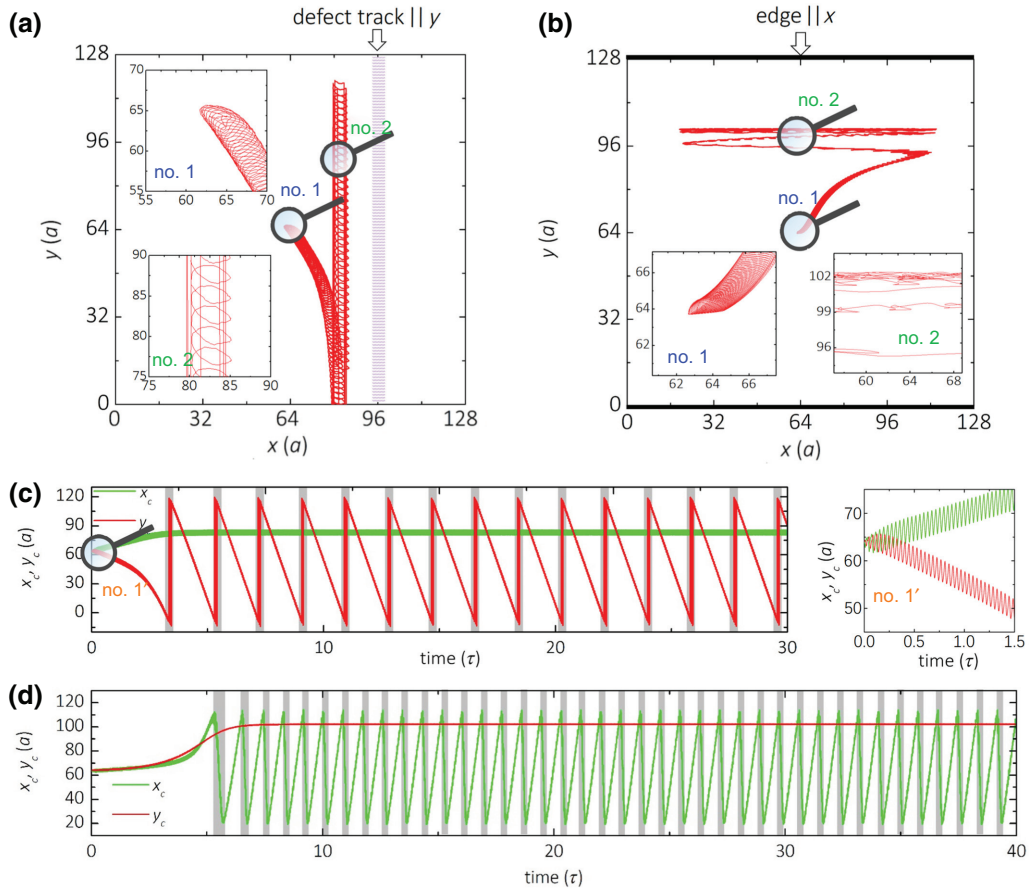


FIG. 2. Long-time defect-mediated skyrmion ratchet motion under a biharmonic in-plane magnetic field $H_x(t) = 0.003[\sin(\omega t) + \sin(2\omega t)]$. (a) Trajectory of a skyrmion moving toward and along a $4a$ -wide defect track ($\eta_{\text{DMI}} = 0.5$) parallel to the y axis (denoted as “defect track $\parallel y$ ”) and locating at $x = 96a$. (b) Trajectory of a skyrmion moving toward and along an edge parallel to the x axis (denoted as “edge $\parallel x$ ”) and locating at $y = 128a$. For both cases, the skyrmion is initially located at position $(64a, 64a)$, which is far enough from the defect track and edge, so that the skyrmion motion therein can be considered as in the bulk region. (c) Long-time evolution curves of the skyrmion position coordinate y_c of case “defect track $\parallel y$.” (d) Long-time evolution curves of the skyrmion position coordinate x_c of the case “edge $\parallel x$.”

Figs. 2(c) and 2(d), respectively. It shows that the y_c curve of case “defect track $\parallel y$ ” and the x_c curve of case “edge $\parallel x$ ” have smooth slopes at the beginning of several nanoseconds (the unit of time τ is about 1.5 ns, see Sec. II). This corresponds to the stage of skyrmion approaching the defect track or the edge. Then, the curves show periodic zigzags with steep slopes, corresponding to the stage of a fast ratchet motion along the defect track or the edge. Note, due to the use of periodic boundary conditions, here each zigzag of the y_c or x_c curve corresponds to a $128a$ displacement of the skyrmion, and the period of the zigzag is the time for the skyrmion to move over 128 lattices. One can readily estimate the ratchet motion speed v_c along the defect track and the edge to be about $68.7a/\tau$ and $147.9a/\tau$, respectively. For a typical value of $a = 1$ nm, the speed values are 45.8 m/s and 98.6 m/s, respectively, which are comparable to that driven by currents. On the other hand, from the slope of the y_c or x_c curve at the beginning [see,

e.g., in the “no. 1” inset in Fig. 2(c)], the ratchet motion speed in the bulk region is about $9.54 a/\tau$ (i.e., 6.4 m/s for $a = 1$ nm). This result shows that the speed-up effect of defect track and edge on the skyrmion ratchet motion is remarkable, with a factor over 10.

To clearly see the change of skyrmion configuration under the biharmonic in-plane field and the effect of defect, in Fig. 3 we depict the snapshots of the contour map of m_z during the motion of skyrmion towards and along the edge (case “edge $\parallel x$ ”). The movies of skyrmion ratchet motion along the defect track (“defect track $\parallel y$ ”) and the edge (“edge $\parallel x$ ”) are further provided in the Supplemental Material [43]. A detailed analysis on the characteristics of such a skyrmion ratchet motion in the time domain and frequency domain is also shown in Fig. S4 within the Supplemental Material [43]. One can see from these results that, under the driving force of the biharmonic field, the skyrmion is excited into a CCW gyration mode in the bulk

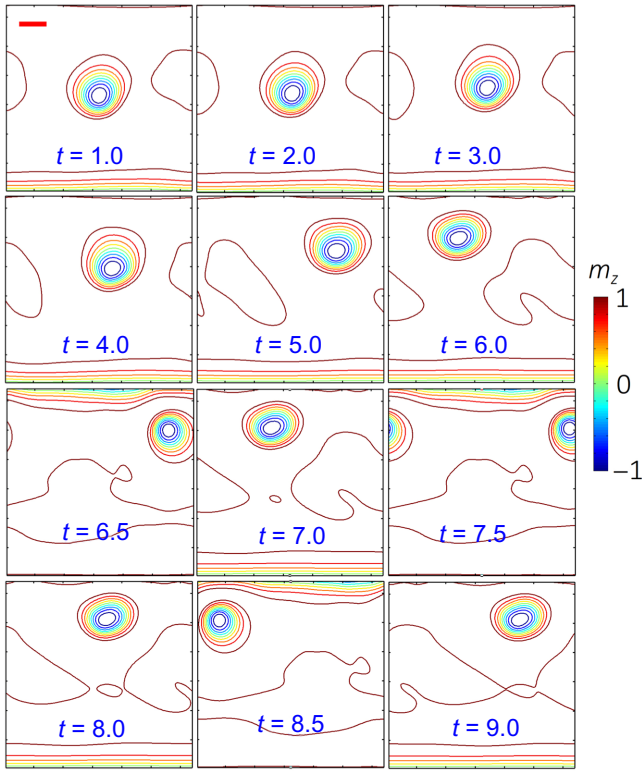


FIG. 3. Snapshots of the contour map of m_z of skyrmion during ratchet motion towards and along an edge parallel to the x axis (case “edge $\parallel x$ ”) under a biharmonic field $H_x(t) = 0.003[\sin(\omega t) + \sin(2\omega t)]$. The length bar in red is $20a$.

region with a significant time-varying deformation. While the skyrmion is still in a CCW gyration mode when it is moving along the defect track (“defect track $\parallel y$ ”) as can be seen in Fig. 2(a), the motion trajectory of skyrmion is more complicated when it is moving along the edge (“edge $\parallel x$ ”), implying a strong effect of the skyrmion-edge interaction [see Figs. 2(b) and S4 within the Supplemental Material [43]]. From the frequency spectrum of skyrmion ratchet motion shown in Fig. S4 within the Supplemental Material [43], one can also see that multimodes of frequencies ω , 2ω , 3ω , ..., are all excited, implying a nonlinear feature of the skyrmion dynamics. Moreover, when the skyrmion approaches the edge or defect track, it shows a slight shrinkage along the direction perpendicular to the edge or defect track, implying that the skyrmion is subjected to a repulsive force from the edge or defect track.

B. Facile control on the defect-induced ultrafast ratchet motion of skyrmion

Note, by varying the phase φ of the biharmonic field in form of $H_x(t) = h_1 \sin(m\omega t) + h_2 \sin(n\omega t + \varphi)$, direction of the skyrmion ratchet motion in the bulk region (i.e., where skyrmion is far away enough from defect tracks or edges) can be continuously rotated by 360° as shown in Fig. S5

within the Supplemental Material [43]. Consequently, skyrmion will be driven towards and along or away from a defect track or edge, depending on the phase φ of the biharmonic field. This 360° ratchet motion of skyrmion controllable by the phase φ is an analogy to the 360° direct motion of skyrmion by controlling the magnetization direction of the spin current injected in the out-of-plane direction [19], and it is potentially useful in driving skyrmions in insulating systems. Double-track or double-edge structures can be further designed to confine the skyrmion ratchet motion within the region between double defect tracks or double edges, acting like racetrack-type highways of skyrmion ratchet motion. In the following, we discuss the influence of phase φ on the skyrmion ratchet motion within a double-track structure under biharmonic in-plane magnetic fields $H_x(t) = 0.003[\sin(\omega t) + \sin(2\omega t + \varphi)]$ with φ varying from 0 to 360° . In the simulated $128a \times 128a$ spin-lattice system, two $4a$ -wide defect tracks (parallel to the y axis, $\eta_{\text{DMI}} = 0.5$) are located at $x = 32a$ and $x = 96a$. For a given φ , an isolating skyrmion is initially located at position $(64a, 64a)$.

The long-time evolution curves of the position coordinate y_c and the corresponding trajectories of skyrmion ratchet motion at various phase φ are depicted in Figs. 4(a) and 4(b), respectively. One can see from the number of the zigzags in the y_c curves in Fig. 4(a) that the ratchet motion speed of skyrmion along the defect track is sensitive to phase φ . In addition, although the direction of the skyrmion ratchet motion in the bulk region is 360° rotatable (see Fig. S5 within the Supplemental Material [43]), the skyrmion is finally either in upward ratchet motion along the left defect track $\parallel y$ or in downward ratchet motion along the right defect track $\parallel y$ as shown in Fig. 4(b). That is to say, the ratchet motion of skyrmion along the defect track has a fixed direction (which can be represent by $\mathbf{e}_z \times \mathbf{e}_d$, with \mathbf{e}_z being the vector along out-of-plane direction and \mathbf{e}_d being the vector perpendicular to the defect track and pointing to the skyrmion), no matter the skyrmion has an initial upward or downward velocity when it approaches the defect track. This indicates the skyrmion is subjected to an effective repulsive force (fixed in direction \mathbf{e}_d) from the defect track, and the force plays a role in the ratchet motion of skyrmion.

The skyrmion ratchet-motion speed and the speed-up factor as a function of phase φ are calculated and depicted in Fig. 4(c), both for motion along the defect track and in the bulk region. Here, the speed along the defect track v is plotted with a plus or minus sign, denoting the upward motion along the left defect track or downward motion along the right defect track. Moreover, the speed-up factor is defined as the ratio between the ratchet motion speed along the defect track (determined by the slope of the zigzag) and that in the bulk region (determined by the slope of the y_c curves at the beginning 1 ns). One can see that both the ratchet motions in the bulk region and along

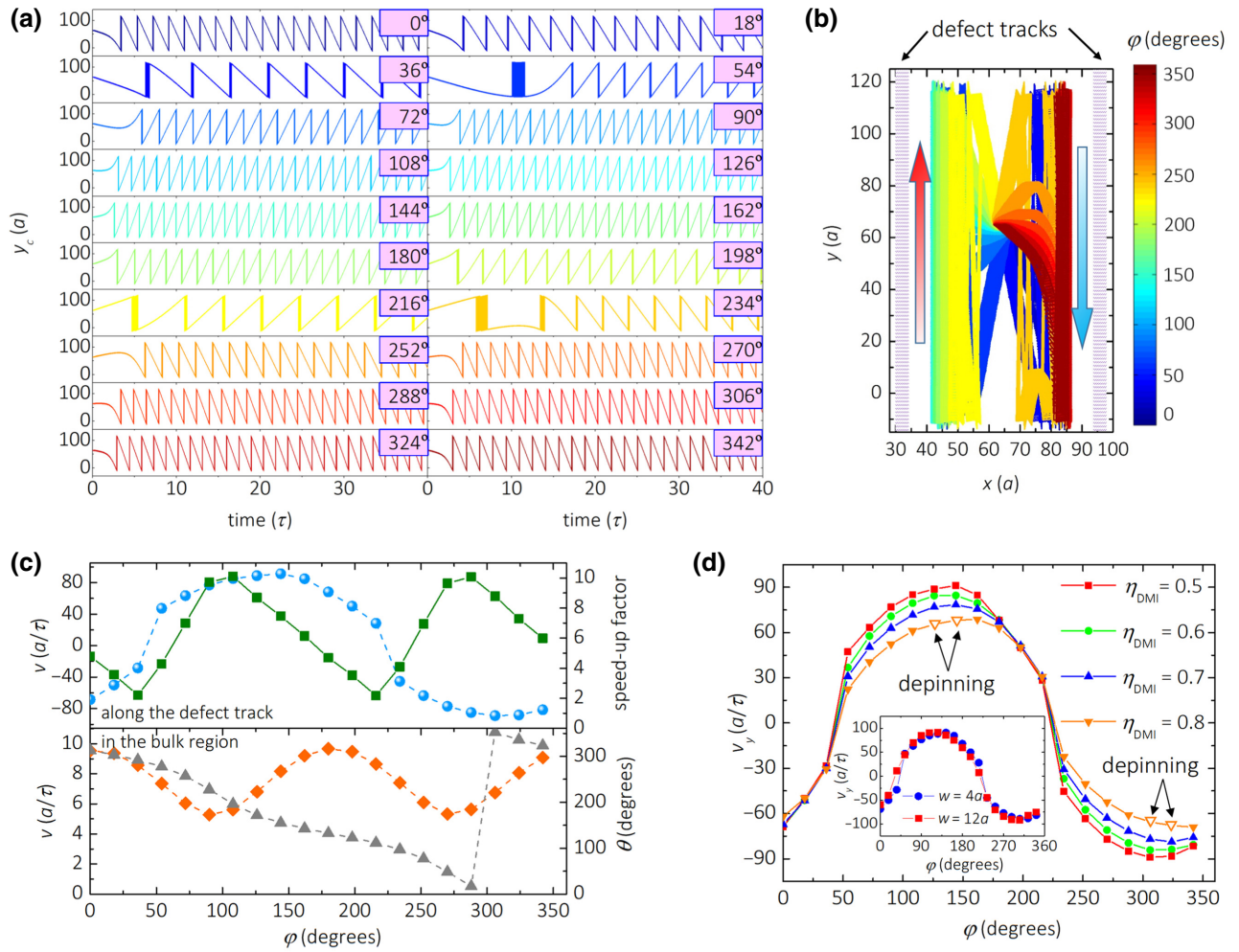


FIG. 4. The influence of phase φ on the skyrmion ratchet motion along defect tracks $\parallel y$ under biharmonic in-plane magnetic fields $H_x(t) = 0.003[\sin(\omega t) + \sin(2\omega t + \varphi)]$. (a) Long-time evolution curves of the position coordinate y_c of skyrmion ratchet motion controlled by phase φ . In the simulation box, two $4a$ -wide defect tracks (parallel to the y axis, $\eta_{DMI} = 0.5$) are located at $x = 32a$ and $x = 96a$. For a given φ , the skyrmion is initially located at position $(64a, 64a)$ and the skyrmion motion at the beginning can be considered as in the bulk region. Under the driving of $H_x(t)$, the skyrmion will be finally either in upward ratchet motion along the left defect track $\parallel y$ or in downward ratchet motion along the right track $\parallel y$, depending on the value of phase φ . (b) Trajectories of skyrmion ratchet motion at various phase φ . (c) Comparison of the skyrmion ratchet-motion velocity along the defect track $\parallel y$ and in the bulk region. The speed-up factor is denoted as the ratio of the ratchet-motion speed along the defect track to that in the bulk region. It is an oscillating function of phase φ in period of 180° with a maximum value of approximately 10 as shown in the up panel. (d) Skyrmion ratchet speed v_y as a function of phase φ of the biharmonic field for the case of “defect track $\parallel y$ ” with different defect strength η_{DMI} . Effect of the width of defect track is shown in the inset. Note, depinning occurs once the force perpendicular to the defect track exceeds the depinning force but the defect strength is not strong enough ($\eta_{DMI} = 0.8$).

the defect track are tunable by phase φ . The v - φ curves are sinusoidal-like, with a near 40° difference between the peaks of the ratchet-motion speed along the defect tracks and that of the bulk region. The maximum ratchet-motion speed along the defect tracks is about $91.3a/\tau$ at φ around 130° (downward along the right track) and 310° (upward along the left track), whereas the maximum ratchet-motion speed in the bulk region is about $9.5 a/\tau$ at φ around 0° and 180° . The maximum speed-up factor is over 10 at φ around 105° and 285° , and the minimum speed-up factor is about 2.2 at φ around 35° and 215° .

The φ -dependent speed-up effect of the skyrmion ratchet motion along the defect track can be further modified by the defect parameters. Figure 4(d) depicts the skyrmion ratchet speed v_y as a function of phase φ of the biharmonic field for cases with different defect strength η_{DMI} . Effect of the width of defect track w is also shown in the inset. It can be seen that the ratchet-motion speed is more sensitive to the defect strength than the width of defect track, implying the dominant effect comes from the border of the defect track. The defect strength mainly affects the ratchet motion speed rather than shifting the v - φ curve along the

φ axis. With the change of the defect strength η_{DMI} from 0.8 to 0.5, the maximum ratchet-motion speed increases from about $68.5a/\tau$ to $91.3a/\tau$ (by a factor of approximately 1.3). Moreover, depinning occurs when the defect strength is not strong enough ($\eta_{\text{DMI}} = 0.8$), indicating that the effective driving force exerted to the skyrmion exceeds the depinning force of the defect track. The change of the width of defect track from $w = 4a$ to $12a$ slightly shifts the v - φ curve by approximately 15° , with a minor effect on the maximum speed.

To clearly see the effect of phase φ on the skyrmion ratchet motion along the defect track, we depict the polar graphs of the skyrmion ratchet-motion speed and the speed-up factor as a function of phase φ [Figs. 5(a) and 5(b)]. The polar curves of ratchet-motion speed are in peanut-shape with two peaks and valleys. The polar curve of ratchet-motion speed along the defect tracks have a near 40° rotation with those of the bulk region [Fig. 5(a)]. As a result, the polar curve of the speed-up factor shows a distortion from that of the speed curve [Fig. 5(b)]. Note, the motion angle θ , defined as the angle between the velocity vector and the x axis, is 360° rotatable with the change of phase φ when the skyrmion moves in the bulk region [Fig. 4(c)]. By plotting the polar graphs of the

ratchet-motion speed and the speed-up factor as a function of the motion angle θ in the bulk region (Fig. S6 within the Supplemental Material [43]), one can see that the fastest ratchet motion along the defect track actually occurs when θ is about 0 and 180° , that is, when the skyrmion is perpendicularly incident to the defect track. For this motion angle, the repulsive force of the defect track should be maximum, implying the useful role of the repulsive force of the defect track in the ultrafast ratchet effect.

Skyrmion ratchet motion along the edge driven by biharmonic in-plane magnetic fields is found to be much less sensitive to phase φ than the case of motion along defect track (see Figs. S7 and S8 within the Supplemental Material [43]). In the simulation, there are two open edges at the two boundaries of the lattice systems parallel to the x axis as that shown in Fig. 2(b). With phase φ changing from 0° to 360° , the direction of the skyrmion ratchet motion is either in rightward motion along the upper edge or in leftward motion along the bottom edge. Moreover, the ratchet motion speed along the edge is generally large, which is about $150 a/\tau$ for all φ and is about 1.7 times of the maximum speed moving along the defect track (approximately $90 a/\tau$). For this case, as the phase sensitivity of the ratchet-motion speed is rather weak, it would be more efficient to tune the ratchet-motion speed along the edge by controlling the field strength of the biharmonic field, or by controlling the pulse width of pulsed magnetic fields as shown in Fig. 6. Here, the pulsed fields $H_x(t)$ are repetitive sequences of alternating positive pulse over a time TN_1 and negative pulse over a time TN_2 [Fig. 6(a)]. The field strength of the positive and negative pulses is 0.003 in reduced unit (approximately 33 mT), and $TN_1 + TN_2 = TN$ is fixed to be 0.04τ (approximately 60 ps). From the long-time evolution curves of the position coordinate x_c of skyrmion ratchet motion under pulsed fields with different TN_1 [Fig. 6(b)], one can see that the skyrmion ratchet-motion speed along the edge significantly increases with the change of TN_1 from 0.002τ to 0.01τ . The facile control of the ratchet-motion speed by pulsed fields is believed to be caused by the resonance effect and is practically useful for driving skyrmion in nanotracks with open edges.

C. Mechanism analysis of the defect-induced ultrafast ratchet motion of skyrmion

To understand the origin of the defect-induced ultrafast ratchet motion of skyrmion, we further analyze the skyrmion motion based on the time-averaged Thiele equation $\mathbf{G} \times \mathbf{v} + \overleftrightarrow{\mathbf{D}} \cdot \mathbf{v} = \mathbf{F}$ as derived in Sec. II B, where \mathbf{v} and \mathbf{F} are the time-averaged velocity and effective driving force over a period, and \mathbf{G} and $\overleftrightarrow{\mathbf{D}}$ being the effective gyromagnetic vector and the dissipative force tensor determined by the time-averaged magnetization over a period, respectively. The effective driving force \mathbf{F} should include the contributions of the external field, the

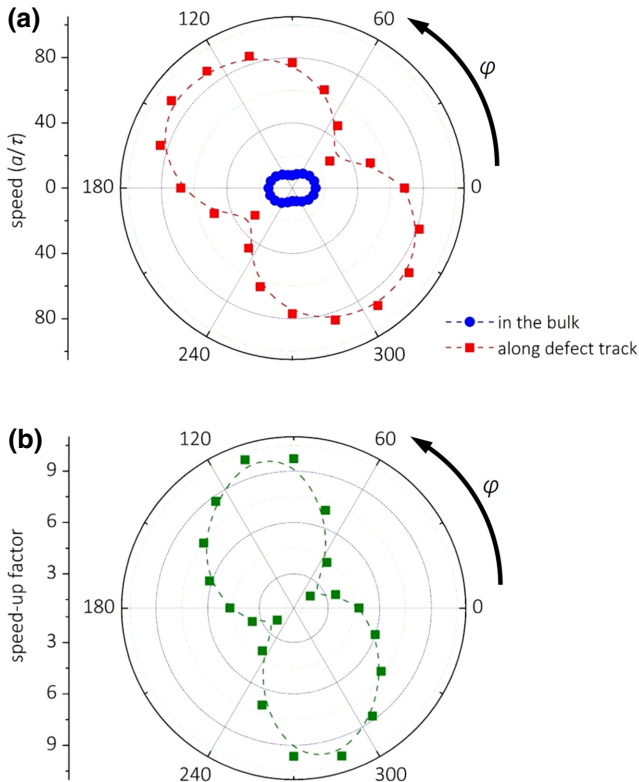


FIG. 5. (a) Skyrmion ratchet motion speed and (b) speed-up factor as a function of phase φ for skyrmion ratchet motion along defect tracks $\parallel y$ under biharmonic magnetic fields $H_x(t) = 0.003[\sin(\omega t) + \sin(2\omega t + \varphi)]$.

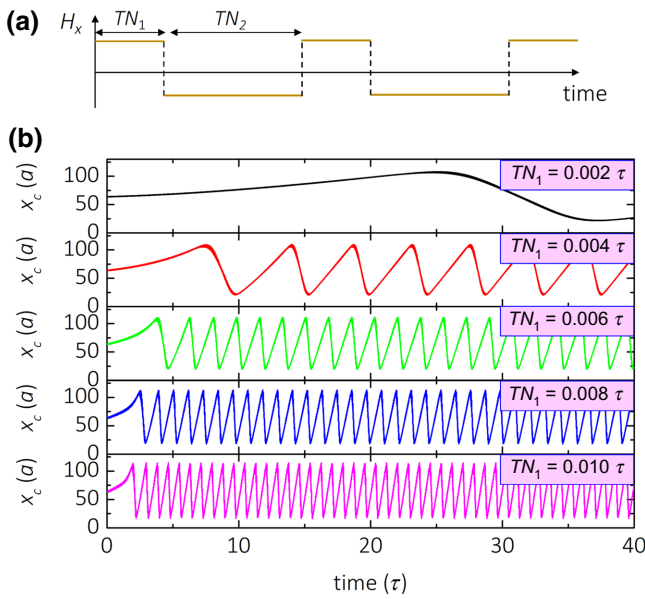


FIG. 6. Ultrafast skyrmion ratchet motion along an edge $\parallel x$ under pulsed in-plane magnetic fields. (a) Schematic of the pulsed magnetic fields $H_x(t)$, which are repetitive sequences of alternating positive pulse over a time TN_1 and negative pulse over a time TN_2 . (b) Long-time evolution curves of the position coordinate x_c of skyrmion ratchet motion at various TN_1 . Here, the magnitudes of the positive and negative pulses are $0.003J/g\mu_B$, and $TN_1 + TN_2 = TN$ is fixed to be 60ps .

skyrmion-magnon interaction, as well as the skyrmion-defect interaction or the skyrmion-edge interaction. However, a physically rigorous separation of these contributions is difficult as the skyrmion deforms during the ratchet motion. While one may still imagine the skyrmion during the ratchet motion as a rigid particle with an ideal circular shape embedded in the flux of magnons, the uncertainty of the skyrmion position during the ratchet motion can lead to a problematic separation of the magnetization fields of the skyrmion and magnons. Alternatively, one may associate the skyrmion during the ratchet motion with a steady deformation defined by the time-averaged magnetization \mathbf{m}_0 . Then, the effective driving force \mathbf{F} would be decomposed into a “deformation force” $\mathbf{F}_{\mathbf{m}_0}$ related to the steady skyrmion deformation during the ratchet motion, and a “dynamic force” $\mathbf{F}_{\mathbf{n}}$ related to the spin waves (magnons) dynamics as shown in Eqs. (16)–(18).

Figure 7(a) depicts the snapshots of the density map of the effective driving force \mathbf{F} when a skyrmion moves toward and along an edge parallel to the x axis under a biharmonic in-plane magnetic field $H_x(t) = 0.003[\sin(\omega t) + \sin(2\omega t)]$ with $\omega = 105\text{ Grad/s}$. The simulation setting is the same as that in Fig. 2. One can see that the force density takes large values mainly near the skyrmion. When the skyrmion approaches the edge, the force changes direction from being lower right

to being perpendicular to the edge and shows a remarkable increase in magnitude as indicated by the ranges of the color bars. To see the difference between the driving forces subjected by the skyrmion when it moves in the bulk region and along the defect track or the edge, we further depict in Fig. 7(b) the evolution curves of effective driving force components $F_{x(y)}$ subjected by skyrmion under biharmonic field $H_x(t) = 0.003[\sin(\omega t) + \sin(2\omega t)]$ with $\omega = 105\text{ Grad/s}$. For the cases of “defect track $\parallel y$ ” and “edge $\parallel x$,” the simulation settings are the same as those in Fig. 2. The evolution curves of $\mathbf{F}_{\mathbf{m}_0}$, $\mathbf{F}_{\mathbf{n}}$ and the force related to the magnon currents $\mathbf{F}_{\text{magnon}}$ of the three cases are further depicted in Figs. S9 to S11 within the Supplemental Material [43]. From these results, the effective driving force is small for ratchet motion without defect tracks or edges (case “bulk”) or far from the defect tracks or edges (cases “defect track $\parallel y$ ” and “edge $\parallel x$ ” at the beginning). The effective driving force remarkably increases as the skyrmion approaches the defect track or edge. The contributions of $\mathbf{F}_{\mathbf{m}_0}$ and $\mathbf{F}_{\mathbf{n}}$ to the effective force \mathbf{F} are in similar order for the first two cases, whereas $\mathbf{F}_{\mathbf{m}_0}$ is much larger than $\mathbf{F}_{\mathbf{n}}$ for the case of “edge $\parallel x$.” Moreover, the direction of $\mathbf{F}_{\mathbf{m}_0}$ is approximately perpendicular to the defect track for the case of “defect track $\parallel y$,” whereas the direction of $\mathbf{F}_{\mathbf{m}_0}$ is approximately perpendicular to edge for the “edge $\parallel x$.” This implies the usefulness of the skyrmion-defect interaction and the skyrmion-edge interaction in the “deformation force” $\mathbf{F}_{\mathbf{m}_0}$. Note also that $\mathbf{F}_{\text{magnon}}$ is largest (smallest) for the case “edge $\parallel x$ ” (“bulk”), indicating the role of magnon excitation in the fast ratchet motion. At steady motion, the effective driving force is found to be (in units of a/τ) $\mathbf{F} = (F_x, F_y) = (-72.6, -62.5)$ for case “bulk,” $(-545.6, -49.4)$ for the case “defect track $\parallel y$,” and $(104.4, -1367.3)$ for case “edge $\parallel x$,” respectively. According to these values, we estimate the ratchet motion speed v and motion angle θ of the three cases based on the approximated relation $\mathbf{G} \times \mathbf{v} \sim \mathbf{F}$ and $\mathbf{G} \sim -4\pi \mathbf{e}_z$. This gives $v = 7.6a/\tau$ and $\theta = 310.7^\circ$ for the case “bulk,” $v = 43.6a/\tau$ and $\theta = 275.2^\circ$ for the case “defect track $\parallel y$,” and $v = 109.1a/\tau$ and $\theta = 4.4^\circ$ for the case “edge $\parallel x$.” These estimated values are in good consistency with the simulation results, verifying the correctness of our physical picture. Therefore, it can be concluded that the speed-up effect of skyrmion ratchet motion by defect track or edge is caused by the remarkable increase of the effective driving force perpendicular to the skyrmion motion when it approaches the defect track or the edge [Fig. 7(c)].

Note, there are actually various situations when a skyrmion encounters the defect track or edge as schematically shown in Fig. 7(d). Depending on the relative magnitudes of the force perpendicular to the defect track or edge F subjected by skyrmion and the critical force F_c of depinning or annihilation, three situations of skyrmion motion can happen: (i) skyrmion moves along the defect

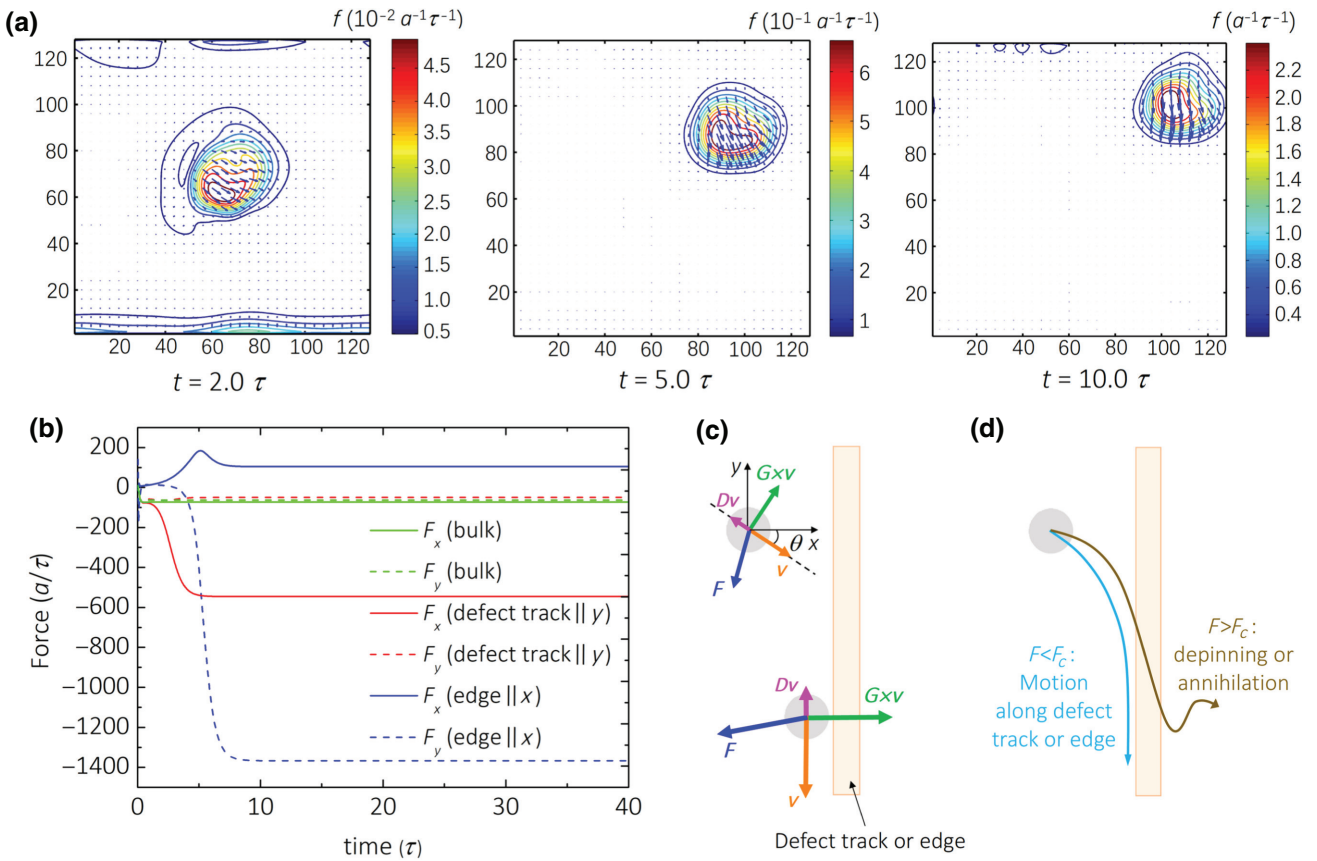


FIG. 7. Force analysis of the defect-induced ultrafast ratchet motion of skyrmion under biharmonic in-plane magnetic fields $H_x(t) = 0.003[\sin(\omega t) + \sin(2\omega t + \varphi)]$. (a) Snapshots of the force density map of skyrmion moving toward and along an edge $\parallel x$. (b) Evolution of time-averaged driving force components $F_{x(y)}$ subjected by skyrmion when it moves in the bulk region (denoted as “bulk”), along a defect track parallel to the y axis (denoted as “defect track $\parallel y$ ”), and along an edge parallel to the x axis (denoted as “edge $\parallel x$ ”). For all the cases, the box size is $128a \times 128a$, and skyrmion is initially located at position $(64a, 64a)$. For the case of “defect track $\parallel y$,” the defect track is $4a$ -wide with $\eta_{\text{DMI}} = 0.5$ and located at $x = 96a$. For the case of “edge $\parallel x$,” the edge is located at $y = 128a$. (c) Schematic of the forces subjected by a skyrmion when it is moving in the bulk region and along a defect track or edge. (d) Schematic illustration of two situations when a skyrmion encounters a defect track or edge. Depending on the relative magnitudes of the force perpendicular to the defect track or edge F subjected by skyrmion and the critical force F_c of depinning or annihilation, three situations of skyrmion motion are expected: (i) skyrmion moves along the defect track or edge ($F < F_c$), (ii) passes through the defect track ($F > F_c$ of depinning), and (iii) annihilates at the defect track or edge ($F > F_c$ of annihilation).

track or the edge ($F < F_c$), (ii) passes through the defect track ($F > F_c$ of depinning), and (iii) annihilates at the defect track or the edge ($F > F_c$ of annihilation). The effective force of a defect track or an edge exerted to the skyrmion undergoing ratchet motion depends on the distance between the skyrmion and the defect track or edge and the defect parameters (e.g., the defect strength and track width), similar to the cases of interactions between skyrmion and defect track or edge without significant excitation [44]. However, for the ratchet motion, the skyrmion-magnon interaction also contributes to the effective force of a defect track or an edge exerted to the skyrmion [Eq. (16)]. F_c of depinning should be also a function of the defect parameters, whereas F_c of annihilation is affected by the skyrmion stability [45]. For example, the result shows that depinning does not occur when

skyrmion moves along a defect track $\parallel y$ with $\eta_{\text{DMI}} = 0.5$ under driving field $H_x(t) = 0.003[\sin(\omega t) + \sin(2\omega t + \varphi)]$, but occurs when skyrmion moves along a defect track $\parallel y$ with $\eta_{\text{DMI}} = 0.8$ when $\varphi = 135^\circ$ as shown in Fig. 4(d). For such a defect track, F_c of depinning is found to be about $270a/\tau$. For skyrmion ratchet motion along an edge $\parallel x$, annihilation occurs under a larger driving field $H_x(t) = 0.0035[\sin(\omega t) + \sin(2\omega t)]$, and F_c of annihilation is about $1160a/\tau$.

Based on the above force analysis, we can further explain the controllability of the speed-up effect along the defect track or edge by the field and defect parameters. Take the skyrmion ratchet motion along defect track $\parallel y$ and along edge $\parallel x$ under biharmonic fields $H_x(t) = 0.003[\sin(\omega t) + \sin(2\omega t + \varphi)]$ as an example. In previous results, we have shown that the ratchet-motion

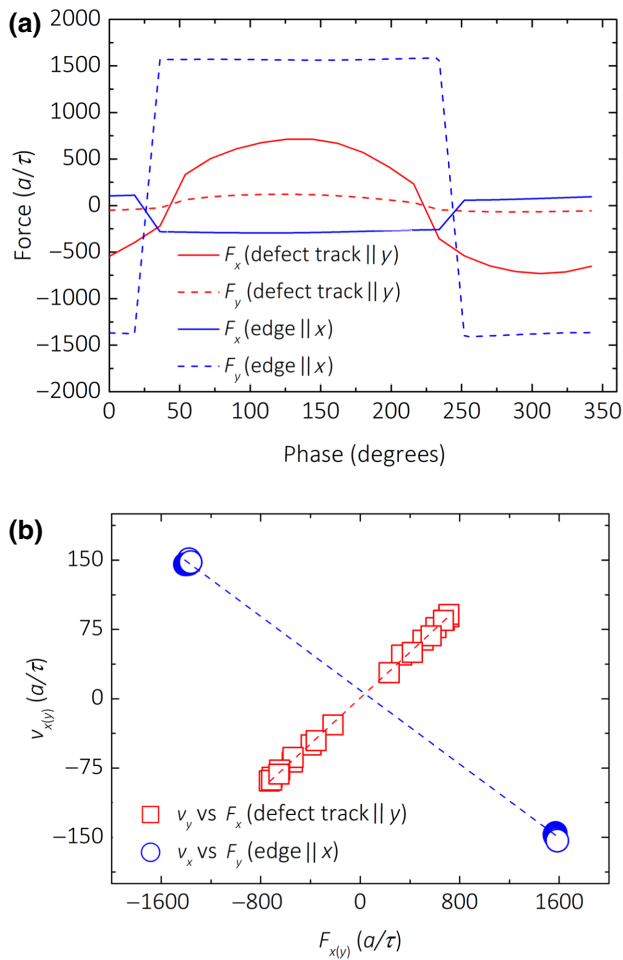


FIG. 8. Force analysis of the defect-induced ultrafast ratchet motion of skyrmion under biharmonic in-plane magnetic fields $H_x(t) = 0.003[\sin(\omega t) + \sin(2\omega t + \varphi)]$. (a) Time-averaged driving force components $F_{x(y)}$ subjected by skyrmion as functions of phase φ for cases of “defect track || y” and “edge || x.” (b) Correlation between the skyrmion ratchet speed $v_{x(y)}$ and force $F_{x(y)}$ for cases of “defect track || y” and “edge || x.”

speed along the defect track is highly tunable by phase φ (Fig. 4), meanwhile the ratchet motion along the edge is much less sensitive to phase φ (Figs. S7 and S8 within the Supplemental Material [43]). For these two cases, the different φ sensitivity of the ratchet-motion speed is due to the different φ dependences of the effective driving force \mathbf{F} as shown in Fig. 8(a). One can see that the force curves of the two cases are highly consistent with the speed curves [Figs. 4(c) and S8 within the Supplemental Material [43]]. The force curves of case “defect track || y” is much smoother than that of the case “edge || x.” Moreover, it is clearly seen from the force curves of case “defect track || y” that the peak and valley values of the ratchet-motion speed correspond to the maximum and minimum values of F_x . Figure 8(b) further shows a plot of the skyrmion ratchet speed as a function of driving force based on the data of

Fig. 8(a). A clear linear correlation between speed and force is seen from the data of “defect track || y,” in consistency with the approximated relation $\mathbf{G} \times \mathbf{v} \sim \mathbf{F}$. From the slopes of $v_{x(y)}$ vs $F_{x(y)}$ curves, one can estimate the magnitude of the “effective” gyromagnetic vector \mathbf{G} is about 8 and 10 for the cases of “defect track || y” and “edge || x,” respectively. These values are smaller than 4π , implying the difference between the time-averaged magnetization of skyrmion during ratchet motion and that at the equilibrium.

At the end of this part, we point out that the ultrafast ratchet motions can be realized by defect tracks, which have different exchange interaction or anisotropy from those at the bulk region (Figs. S12 and S13 within the Supplemental Material [43]). The ratchet motion along such defect tracks is also highly tunable by the field parameters and the defect strength. Moreover, ultrafast ratchet motions also occur along nonstraight edges (with an angular velocity being over 10^9 rad/s) and the skyrmion can easily turn around and follow the corner of the edge, as indicated by our simulations of skyrmion ratchet motion along the edges of a circular disk and a square dot (see Figs. S14 and S15 within the Supplemental Material [43], respectively). More complicated motions of skyrmion can be realized by proper defect engineering, geometrical designing, control of the field parameters, and the involvement of skyrmion-skyrmion interactions. The mechanism is also applicable for Néel-type skyrmions as shown in Fig. S16 within the Supplemental Material [43]. All these suggest a promising way to control skyrmions for devices.

IV. CONCLUSIONS

Via massive micromagnetic simulations and analytical modeling, we reveal the ultrafast ratchet dynamics of skyrmion by defect engineering under gigahertz magnetic fields. It is found that the ratchet motion of skyrmion is not only guided along the defect tracks or edges, but also with a remarkable speed up (with a factor over 10) compared with that in the bulk region. The skyrmion ratchet-motion speed and direction along the defect track or edge can be facily controlled by the field and defect parameters. The skyrmion ratchet-motion speed along a straight defect track or edge a field of approximately 50 mT is comparable to the direct motions (approximately 100 m/s) driven by currents. The speed-up effect is due to the increased effective driving force perpendicular to the skyrmion motion when it approaches the defect track or edge.

The reported ultrafast skyrmion ratchet motion is a conjoint effect of the solitonlike feature of magnetic skyrmions and skyrmion-defect interaction or the skyrmion-edge interaction. The driving sources can be magnetic fields or other time-varying sources with gigahertz characteristic frequencies rather than spin-polarized currents. As shown by our results, magnetic fields of about 50 mT can trigger efficient ratchet motion along defect tracks

or edges in a speed of about 100 m/s. Note, the presence of defects or edges in the skyrmion system lowers the spatial symmetry of the system, and ratchet motion of skyrmion along a defect track or edge can actually be induced by time-varying sources without time asymmetry [46,47]. The mechanism reported in our work therefore provides a general and feasible strategy to efficiently drive skyrmion in both metallic and insulating systems based on racetrack structures. Our conclusions can be extended to other Magnus-dominated particle systems. So far what we explore is the ratchet motion of a single skyrmion, it is interesting to further explore the ratchet motion of multiple-skyrmion systems under biharmonic fields with the presence of skyrmion-skyrmion interactions. For such systems, more complicated motion modes can appear (e.g., the two skyrmions rotate around each other like a binary star system simultaneously with a slow ratchet speed as shown in Fig. S17 within the Supplemental Material [43]). We would like to investigate this issue in the near future.

ACKNOWLEDGMENTS

The authors gratefully acknowledge the financial support of National Natural Science Foundation of China (Grants No. 11972382, No. 11672339, and No. 11832019), Guangzhou Science and Technology Project (Grant No. 201707020002), and Fundamental Research Funds for the Central Universities.

-
- [1] Y. Zheng and W. J. Chen, Characteristics and controllability of vortices in ferromagnetics, ferroelectrics, and multiferroics, *Rep. Prog. Phys.* **80**, 086501 (2017).
- [2] N. Nagaosa and Y. Tokura, Topological properties and dynamics of magnetic skyrmions, *Nat. Nanotechnol.* **8**, 899 (2013).
- [3] A. Fert, N. Reyren, and V. Cros, Magnetic skyrmions: Advances in physics and potential applications, *Nat. Rev. Mater.* **2**, 1 (2017).
- [4] U. K. Roessler, A. N. Bogdanov, and C. Pfleiderer, Spontaneous skyrmion ground states in magnetic metals, *Nature* **442**, 797 (2006).
- [5] S. Mühlbauer, B. Binz, F. Jonietz, C. Pfleiderer, A. Rosch, A. Neubauer, R. Georgii, and P. Böni, Skyrmion lattice in a chiral magnet, *Science* **323**, 915 (2009).
- [6] W. Münzer, A. Neubauer, T. Adams, S. Mühlbauer, C. Franz, F. Jonietz, R. Georgii, P. Böni, B. Pedersen, M. Schmidt, A. Rosch, and C. Pfleiderer, Skyrmion lattice in the doped semiconductor $\text{Fe}_{1-x}\text{Co}_x\text{Si}$, *Phys. Rev. B* **81**, 041203 (2010).
- [7] C. Pfleiderer, T. Adams, A. Bauer, W. Biberacher, B. Binz, F. Birkelbach, P. Böni, C. Franz, R. Georgii, M. Janoschek, F. Jonietz, T. Keller, R. Ritz, S. Mühlbauer, W. Münzer, A. Neubauer, B. Pedersen, and A. Rosch, Skyrmion lattices in metallic and semiconducting B20 transition metal compounds, *J. Phys.: Condens. Matter* **22**, 164207 (2010).
- [8] T. Adams, A. Chacon, M. Wagner, A. Bauer, G. Brandl, B. Pedersen, H. Berger, P. Lemmens, and C. Pfleiderer, Long-wavelength Helimagnetic Order and Skyrmion Lattice Phase in Cu_2OSeO_3 , *Phys. Rev. Lett.* **108**, 237204 (2012).
- [9] E. Ruff, S. Widmann, P. Lunkenheimer, V. Tsurkan, S. Bordács, I. Kézsmárki, and A. Loidl, Multiferroicity and skyrmions carrying electric polarization in GaV_4S_8 , *Sci. Adv.* **1**, e1500916 (2015).
- [10] S. Heinze, K. Von Bergmann, M. Menzel, J. Brede, A. Kubetzka, R. Wiesendanger, G. Bihlmayer, and S. Blügel, Spontaneous atomic-scale magnetic skyrmion lattice in two dimensions, *Nat. Phys.* **7**, 713 (2011).
- [11] W. Jiang, P. Upadhyaya, W. Zhang, G. Yu, M. B. Jungfleisch, F. Y. Fradin, J. E. Pearson, Y. Tserkovnyak, K. L. Wang, O. Heinonen, S. G. E. te Velthuis, and A. Hoffmann, Blowing magnetic skyrmion bubbles, *Science* **349**, 283 (2015).
- [12] O. Boulle, J. Vogel, H. Yang, S. Pizzini, D. de Souza Chaves, A. Locatelli, T. O. Menteş, A. Sala, L. D. Buda-Prejbeanu, O. Klein, M. Belmeguenai, Y. Roussigné, A. Stashkevich, S. M. Chérif, L. Aballe, M. Foerster, M. Chshiev, S. Auffret, and I. M. Miron, G. gaudin, room-temperature chiral magnetic skyrmions in ultrathin magnetic nanostructures, *Nat. Nanotechnol.* **11**, 449 (2016).
- [13] S. Woo, K. Litzius, B. Krüger, M.-Y. Im, L. Caretta, K. Richter, M. Mann, A. Krone, R. M. Reeve, M. Weigand, P. Agrawal, I. Lemesch, M.-A. Mawass, P. Fischer, M. Kläui, and G. S. D. Beach, Observation of room-temperature magnetic skyrmions and their current-driven dynamics in ultrathin metallic ferromagnets, *Nat. Mater.* **15**, 501 (2016).
- [14] C. Moreau-Luchaire, C. Moutafis, N. Reyren, J. Sampaio, C. A. F. Vaz, N. Van Horne, K. Bouzehouane, K. Garcia, C. Deranlot, P. Warnicke, P. Wohlhüter, J.-M. George, M. Weigand, J. Raabe, V. Cros, and A. Fert, Additive interfacial chiral interaction in multilayers for stabilization of small individual skyrmions at room temperature, *Nat. Nanotechnol.* **11**, 444 (2016).
- [15] L. Wang, Q. Feng, Y. Kim, R. Kim, K. H. Lee, S. D. Pollard, Y. J. Shin, H. Zhou, W. Peng, D. Lee, W. Meng, H. Yang, J. H. Han, M. Kim, Q. Lu, and T. W. Noh, Ferroelectrically tunable magnetic skyrmions in ultrathin oxide heterostructures, *Nat. Mater.* **17**, 1087 (2018).
- [16] K. Y. Meng, A. S. Ahmed, M. Baćani, A.-O. Mandru, X. Zhao, N. Bagués, B. D. Esser, J. Flores, D. W. McComb, H. J. Hug, and F. Yang, Observation of nanoscale skyrmions in $\text{SrIrO}_3/\text{SrRuO}_3$ bilayers, *Nano Lett.* **19**, 3169 (2019).
- [17] J. Iwasaki, M. Mochizuki, and N. Nagaosa, Current-induced skyrmion dynamics in constricted geometries, *Nat. Nanotechnol.* **8**, 742 (2013).
- [18] J. Sampaio, V. Cros, S. Rohart, and A. Fert, Nucleation, stability and current-induced motion of isolated magnetic skyrmions in nanostructures, *Nat. Nanotechnol.* **8**, 839 (2013).
- [19] R. Tomasello, E. Martinez, R. Zivieri, L. Torres, M. Carpentieri, and G. Finocchio, A strategy for the design of skyrmion racetrack memories, *Sci. Rep.* **4**, 6784 (2014).
- [20] Y. H. Liu, Y. Q. Li, and J. H. Han, Skyrmion dynamics in multiferroic insulators, *Phys. Rev. B* **87**, 100402 (2013).

- [21] K. Everschor, M. Garst, B. Binz, F. Jonietz, S. Mühlbauer, C. Pfleiderer, and A. Rosch, Rotating skyrmion lattices by spin torques and field or temperature gradients, *Phys. Rev. B* **86**, 054432 (2012).
- [22] L. Kong and J. Zang, Dynamics of an Insulating Skyrmion Under a Temperature Gradient, *Phys. Rev. Lett.* **111**, 067203 (2013).
- [23] M. Mochizuki, X. Z. Yu, S. Seki, N. Kanazawa, W. Koshibae, J. Zang, M. Mostovoy, Y. Tokura, and N. Nagaosa, Thermally driven ratchet motion of a skyrmion microcrystal and topological magnon hall effect, *Nat. Mater.* **13**, 241 (2014).
- [24] P. Upadhyaya, G. Yu, P. K. Amiri, and K. L. Wang, Electric-field guiding of magnetic skyrmions, *Phys. Rev. B* **92**, 134411 (2015).
- [25] W. Wang, M. Beg, B. Zhang, W. Kuch, and H. Fangohr, Driving magnetic skyrmions with microwave fields, *Phys. Rev. B* **92**, 020403 (2015).
- [26] K. W. Moon, D. H. Kim, S. G. Je, B. S. Chun, W. Kim, Z. Q. Qiu, S.-B. Choe, and C. Hwang, Skyrmion motion driven by oscillating magnetic field, *Sci. Rep.* **6**, 20360 (2016).
- [27] C. Psaroudaki and D. Loss, Skyrmions Driven by Intrinsic Magnons, *Phys. Rev. Lett.* **120**, 237203 (2018).
- [28] C. Wang, D. Xiao, X. Chen, Y. Zhou, and Y. Liu, Manipulating and trapping skyrmions by magnetic field gradients, *New J. Phys.* **19**, 083008 (2017).
- [29] W. Jiang, X. Zhang, G. Yu, W. Zhang, X. Wang, M. B. Jungfleisch, J. E. Pearson, X. Cheng, O. Heinonen, K. L. Wang, Y. Zhou, A. Hoffmann, and S. G. E. te Velthuis, Direct observation of the skyrmion hall effect, *Nat. Phys.* **13**, 162 (2017).
- [30] K. Litzius, I. Lemesh, B. Krüger, P. Bassirian, L. Caretta, K. Richter, F. Büttner, K. Sato, O. A. Tretiakov, J. Förster, R. M. Reeve, M. Weigand, I. Bykova, H. Stoll, G. Schütz, G. S. D. Beach, and M. Kläui, Skyrmion Hall effect revealed by direct time-resolved X-ray microscopy, *Nat. Phys.* **13**, 170 (2017).
- [31] J. Iwasaki, W. Koshibae, and N. Nagaosa, Colossal spin transfer torque effect on skyrmion along the edge, *Nano Lett.* **14**, 4432 (2014).
- [32] X. Zhang, G. P. Zhao, H. Fangohr, J. P. Liu, W. X. Xia, J. Xia, and F. J. Morvan, Skyrmion-skyrmion and skyrmion-edge repulsions in skyrmion-based racetrack memory, *Sci. Rep.* **5**, 7643 (2015).
- [33] A. Fert, V. Cros, and J. Sampaio, Skyrmions on the track, *Nat. Nanotechnol.* **8**, 152 (2013).
- [34] I. Purnama, W. L. Gan, D. W. Wong, and W. S. Lew, Guided current-induced skyrmion motion in 1D potential well, *Sci. Rep.* **5**, 10620 (2015).
- [35] J. Castell-Queralt, L. González-Gómez, N. Del-Valle, A. Sanchez, and C. Navau, Accelerating, guiding, and compressing skyrmions by defect rails, *Nanoscale* **11**, 12589 (2019).
- [36] X. Zhang, Y. Zhou, and M. Ezawa, Magnetic bilayer-skyrmions without skyrmion Hall effect, *Nat. Commun.* **7**, 1 (2016).
- [37] B. Göbel, A. Mook, J. Henk, and I. Mertig, Overcoming the speed limit in skyrmion racetrack devices by suppressing the skyrmion Hall effect, *Phys. Rev. B* **99**, 020405 (2019).
- [38] S. Woo, K. M. Song, X. Zhang, Y. Zhou, M. Ezawa, X. Liu, S. Finizio, J. Raabe, N. J. Lee, S.-I. Kim, S.-Y. Park, Y. Kim, J.-Y. Kim, D. Lee, O. Lee, J. W. Choi, B.-C. Min, H. C. Koo, and J. Chang, Current-driven dynamics and inhibition of the skyrmion Hall effect of ferrimagnetic skyrmions in GdFeCo films, *Nat. Commun.* **9**, 1 (2018).
- [39] C. Reichhardt, D. Ray, and C. J. O. Reichhardt, Magnus-induced ratchet effects for skyrmions interacting with asymmetric substrates, *New J. Phys.* **17**, 073034 (2015).
- [40] X. Ma, C. J. O. Reichhardt, and C. Reichhardt, Reversible vector ratchets for skyrmion systems, *Phys. Rev. B* **95**, 104401 (2017).
- [41] W. J. Chen, L. J. Liu, Y. Ji, and Y. Zheng, Skyrmion ratchet effect driven by a biharmonic force, *Phys. Rev. B* **99**, 064431 (2019).
- [42] M. Mochizuki, Spin-wave Modes and Their Intense Excitation Effects in Skyrmion Crystals, *Phys. Rev. Lett.* **108**, 017601 (2012).
- [43] See Supplemental material at <http://link.aps.org/supplemental/10.1103/PhysRevApplied.14.064014> for additional results.
- [44] C. Navau, N. Del-Valle, and A. Sanchez, Interaction of isolated skyrmions with point and linear defects, *J. Magn. Magn. Mater.* **465**, 709 (2018).
- [45] Q. Sheng, X. L. Liu, W. J. Chen, M. Y. Li, L. J. Liu, and Y. Zheng, Realization of skyrmion subtractor and diverter in a voltage-gated synthetic antiferromagnetic racetrack, *J. Appl. Phys.* **125**, 064502 (2019).
- [46] C. Reichhardt and C. J. O. Reichhardt, Chiral edge currents for ac-driven skyrmions in confined pinning geometries, *Phys. Rev. B* **100**, 174424 (2019).
- [47] C. Reichhardt and C. J. O. Reichhardt, Dynamics of magnus dominated particle clusters, collisions, pinning and ratchets. *Phys. Rev. E* **101**, 062602 (2020).